Microchimica Acta (2018) 185: 471
https://doi.org/10.1007/s00604-018-2994-0

ORIGINAL PAPER

Graphitic carbon nitride quantum dots as an "off-on" fluorescent switch for determination of mercury(II) and sulfide

Xuan Wang[1] · Xuefang Yang[1] · Ning Wang[1] · Junjie Lv[1] · Haojiang Wang[1] · Martin M. F. Choi[2] · Wei Bian[1]

Received: 27 May 2018 / Accepted: 8 September 2018 / Published online: 20 September 2018
© Springer-Verlag GmbH Austria, part of Springer Nature 2018

Abstract

A rapid method has been developed for the determination of Hg(II) and sulfide by using graphitic carbon nitride quantum dots (g-CNQDs) as a fluorescent probe. The interaction between Hg(II) and g-CNQDs leads to the quenching of the blue g-CNQD fluorescence (with excitation/emission peaks at 390/450 nm). However, the fluorescence can be recovered after addition of sulfide such that the "turn-off" state is switched back to the "turn-on" state. The g-CNQDs were fully characterized by transmission electron microscopy, X-ray diffractometry, X-ray photoelectron spectroscopy, Fourier transform infrared spectroscopy, UV-vis absorption and fluorescence spectroscopy. Under the optimal experimental conditions, this probe is highly selective and sensitive to Hg(II). The linear response to Hg(II) extends from 0.20 to 21 μM with a detection limit of 3.3 nM. In addition, sulfide can be detected via the recovery of fluorescence. The linear response range for sulfide species is from 8.0 to 45 μM with a detection limit of 22 nM. The mechanism of the "turn-off-on" scheme is discussed. The methods have been applied to the analysis of spiked tap water, lake water and wastewater samples.

Keywords Graphitic carbon nitride · Quantum dots · Nanomaterial · Fluorescent probe · Stern-Volmer plot · Ion detection · Water analysis · Fluorescence quenching · Fluorescence recovery

Introduction

A large number of ions released from wastewater have become a critical worldwide issue due to the severe hazards to the environment and organisms [1, 2]. Industrial wastes are important sources of Hg^{2+} pollution and exposure to mercury may cause damages to brain, kidney and neurological systems [3–6]. On the other hand, sulfide, as one of the highly toxic anion, irritates mucous membranes and in higher concentration may cause unconsciousness and respiratory paralysis [7, 8]. Conventional analytical techniques for ions detection include atomic absorption spectroscopy, inductively-coupled plasma mass spectrometry, and electrochemistry. These methods either are sensitive and selective but expensive, or are easy to operate but weak in sensitivity and selectivity. Therefore, there is an urgent need to develop novel approaches that are convenient and fast as well as sensitive and selective. So far, fluorescence spectroscopy has been a powerful optical technology that can provide a good flexible, sensitive, and simple detection method [9–12].

Carbon nitride as an organic semiconductor consists of carbon and nitrogen which is a promising candidate in carbon materials for applications in many fields [13, 14]. There are several allotropes of C_3N_4 such as α-C_3N_4, β-C_3N_4, pseudo-cubic C_3N_4, cubic C_3N_4 and g-C_3N_4. The history of carbon nitrides can be traced back to 1834 [15]. However, researchers became interested in it in 1990s owing to that β-C_3N_4 was predicted to have extremely high hardness values [16]. In fact, at ambient conditions, graphitic carbon nitride (g-C_3N_4) is the most stable allotrope among various carbon nitrides nanomaterials. g-C_3N_4 was first applied in water splitting as a metal free conjugated

Electronic supplementary material The online version of this article (https://doi.org/10.1007/s00604-018-2994-0) contains supplementary material, which is available to authorized users.

✉ Wei Bian
sxykdx_bianwei@163.com

[1] Shanxi Medical University, Taiyuan 030001, China

[2] Bristol Chinese Christian Church, c/o Tyndale Baptist Church, 137-139 Whiteladies Road, Bristol BS8 2QG, UK

semiconductor photocatalysis [17, 18]. Since then, researchers have been paying more and more attention to g-C_3N_4. Owing to the strong C-N covalent bonding in-plane direction and weak van der Waals interactions between layered (tri-*s*-) triazine units, g-C_3N_4 can be easily synthesized into bulk, nanosheets, nanotubes, quantum dots or other nanostructures [19, 20]. Furthermore, a new type of fluorescent materials, graphitic carbon nitride quantum dots (g-CNQDs) have gained tremendous attentions. The g-CNQDs emerge as a novel fluorescent probe for biological and environment detection because they show bright fluorescence, good water solubility and biocompatibility, low cost, and low cytotoxicity [21–23]. For instance, Achadu et al. prepared g-CNQDs and their 2,2,6,6-tetramethyl (piperidin-1-yl)oxyl derivatives as a "turn off/on" fluorescence probe for ascorbic acid detection [24]. Yin et al. reported a novel one-pot evaporation-condensation strategy to synthesize g-CNQDs which were used as an efficient probe for Fe^{3+} trace analysis and live-cell imaging [25]. Wang et al. constructed an electrochemiluminescence and fluorescence sensor to detect riboflavin based on the resonance energy transfer between donor g-CNQDs and receptor riboflavin [26].

In this work, we report on the low temperature solid-state synthesis of g-CNQDs. Then g-CNQDs was applied as a fluorescence "off-on" probe for detection of Hg^{2+} and S^{2-} in an aqueous solution. Significant fluorescence quenching of g-CNQDs occurs upon addition of different concentrations of Hg^{2+} while S^{2-} can recover the fluorescence of g-CNQDs. As such, g-CNQDs can serve as an effective fluorescent sensing probe for detection of Hg^{2+} and S^{2-} with high sensitivity and selectivity. The reaction mechanism of the "off-on" process has been preliminarily discussed. Finally, g-CNQDs has been successfully applied to the determination of Hg^{2+} and S^{2-} in various spiked water samples.

Experimental

Materials

Sodium citrate dehydrate, urea, mercuric chloride, sodium sulfide nonahydrate, absolute ethanol were purchased from Aladdin Chemical (Shanghai, China, http://www.aladdin-e.com/). All chemicals of analytical grade reagents were used without further purification.

Apparatus and characterization

Transmission electron microscopic (TEM) image was taken using a JEOL 2010-H TEM (Tokyo, Japan). X-ray photoelectron spectra (XPS) were carried out with an AXIS ULTRADLD X-ray photoelectron spectrometer (Kratos, Tokyo, Japan). X-ray diffraction (XRD) was performed on a D8 Advance power X-ray diffractometer (Bremen, Germany). Fourier transform infrared spectrum (FT-IR) of g-CNQDs was measured on a Varian FT-IR-640 spectrometer (Agilent Technologies, Palo Alto, CA, US). UV–vis absorption and fluorescence spectra of g-CNQDs were recorded on a Metash 6100 U*V*/VIS spectrophotometer (Shanghai, China) and a Hitachi F-4500 spectrofluorometer (Tokyo, Japan), respectively. The fluorescence lifetimes were performed on a FLS920 steady-state transient fluorescence spectrometer (Edinburgh, UK).

Preparation of g-CNQDs

The synthesis of g-CNQDs followed the previous reported procedure with slight modifications [27]. Details of the synthesis are deposited in the Electronic Supporting Material.

"Turn off" detection of mercury(II)

Various concentrations of Hg^{2+} and phosphate buffer (10 mM, pH 8.0) were added to 3.0 mL g-CNQD solutions (25 μL, 6.5 mg/L). Afterwards, the mixture solutions were incubated for 8 min at ambient conditions. Fluorescence emission spectra were recorded at an excitation wavelength of 390 nm and the fluorescence intensities were recorded at excitation/emission wavelengths of 390/450 nm. The slit widths of excitation and emission were both set as 10 nm.

"Turn on" detection of sulfide

The g-CNQDs solution (25 μL, 6.5 mg/L) was mixed with Hg^{2+} (13.3 μM), different concentrations of S^{2-} and phosphate buffer (10 mM, pH 8.0) were added to 3.0 mL and incubated for 6 min. The fluorescence emission spectra were recorded at an excitation wavelength of 390 nm. The fluorescence intensities were recorded at excitation/emission wavelengths of 390/450 nm. The slit widths of excitation and emission were both 10 nm.

Water samples pre-treatment and analysis

The lake water was from Yingze Park of Taiyuan, Shanxi Province, China. Tap water was collected from our laboratory. Wastewater was collected from an industry of Taiyuan city. Lake water and tap water samples were both first filtered and then centrifuged to remove large solids and debris. Wastewater was boiled for 10 min first, filtered through a 0.22-μm membrane filter and diluted to 10 times with phosphate buffer (10 mM, pH 8.0). The analyses of Hg^{2+} and S^{2-} in water samples were performed as described in sections ""Turn off" detection of mercury(II)" and ""Turn on" detection of sulfide".

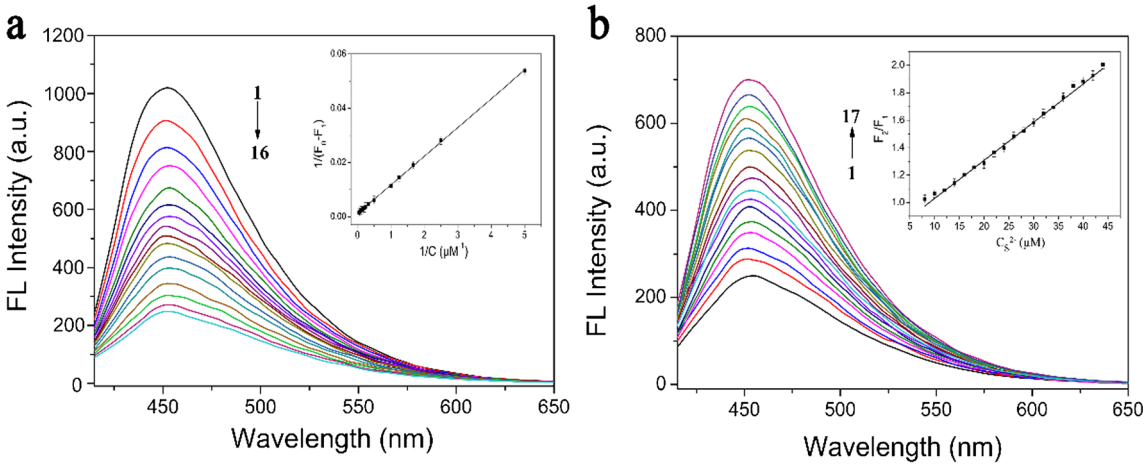

Fig. 1 **a** Effect of Hg^{2+} concentration on the fluorescence spectrum of g-CNQDs. The concentrations of Hg^{2+} are 0.0, 1.2, 2.4, 3.6, 4.8, 6.0, 7.2, 8.4, 9.6, 10.8, 12.0, 13.2, 14.4, 15.6, 16.8, and 18.0 μM from 1 to 16. The inset displays the Lineweaver–Burk plot for the g-CNQDs and Hg^{2+} concentration. **b** Effect of S^{2-} concentration on the fluorescence recovery of g-CNQDs. The concentrations of S^{2-} are 0.0, 8.0, 10.0, 12.0, 14.0, 16.0, 18.0, 20.0, 22.0, 24.0, 26.0, 28.0, 30.0, 32.0, 34.0, 36.0, and 38.0 μM from 1 to 17. The inset displays the linear relationship between the F_2/F_1 and S^{2-} concentration. The excitation and emission wavelength are at 390 and 450 nm, respectively

Results and discussion

Total S(II) concentration in Na_2S solution consists of S^{2-}, HS^- and H_2S. There are two kinds of equilibrium in Na_2S solution:

$$S^{2-} + H^+ \rightleftharpoons HS^-$$
$$HS^- + H^+ \rightleftharpoons H_2S$$

Under acidic conditions, S^{2-} is protonated and converted to HS^- and H_2S. In alkaline condition, the equilibrium shifts to the left due to the existence of more OH^-. Both HS^- and S^{2-} exist in the solution when pH is 8.0 [28–30].

Choice of materials

Fluorescent semiconductor quantum dots (QDs) have shown attractive potential owing to their lots of promising applications, especially in ion detection, cell imaging and biosensing. Nevertheless, the QDs such as CdS and CdSe QDs usually suffer from their toxicity, health and environment hazards because of the heavy metals. Therefore, it is urgent to develop a kind of green, low toxicity, and environmentally QDs. g-CNQDs have attracted much attention because of their simpler synthesis method, low toxicity, good water-solubility, biocompatibility and chemical stability compared with other light-emitting quantum dots.

Characterization of g-CNQDs

The characterization methods for g-CNQDs were measured using TEM, XPS, XRD, FT-IR, UV-visible and fluorescence spectroscopy. Respective data and figures are displayed in the Electronic Supporting Material.

Optimization of method

The following parameters were optimized: (a) Sample pH, (b) Reaction time, (c) Concentration of g-CNQDs (d)

Table 1 An overview on recently reported nanomaterial-based optical methods for the determination of Hg^{2+}

Material	Detection method	LOD	Linear range	Reference
Gold nanorods coated with 6-mercaptopurine	Colorimetry	0.48 nM	1–100 μM	[31]
Exonuclease III/AuNPs	Colorimetry	3.2 pM	0.01–100 μM	[32]
Aptamer-functionalized magnetic beads	Bienzyme-based coloration	0.15 nM	0.5–50 nM	[33]
T-rich DNA aptamer	SERS	10 nM	10 nM–1 mM	[34]
2,4,6-Trimercaptotriazine incorporated gold nanoparticles	Voltammetry	5.3 nM	16–2000 nM	[35]
Nitrogen and sulfur co-doped carbon dots	Fluorescence	6.5 nM	0.01–0.25 μM	[36]
Cysteamine-capped CdTe QDs	Fluorescence	4 nM	6–450 nM	[37]
Silicon nanocrystals	Fluorescence	50 nM	0.05–1 μM	[38]
Graphene quantum dots	Fluorescence	0.1 μM	0.8–9 μM	[39]
g-CNQDs	Fluorescence	3.3 nM	0.2–21 μM	This work

Table 2 An overview on recently reported nanomaterial-based optical methods for the determination of sulfide

Materials	Detection method	LOD	Linear range	Reference
Au nanoparticles	Colorimetry	0.8 μM	0.5–10 μM	[40]
CdS-MAA QDs	Fluorescence	3 nM	0.01–500 μM	[41]
Cu^{2+}-thiamine	Fluorescence	20 nM	0.03–2.5 μM	[42]
Yeast extract-Cu nanoclusters	Fluorescence	10 nM	0.02–0.8 μM	[43]
Cysteine-Cu nanoclusters	Fluorescence	42 μM	0.2–50 μM	[44]
MPA functionalized CdS QDs	Fluorescence	6.5 μM	0.3–55 μM	[45]
Mn-doped ZnS quantum dots	Fluorescence	0.15 μM	2.5–38 μM	[46]
Manganese doped ZnS QDs	Fluorescence	0.33 μM	1.2–26 μM	[47]
g-CNQDs-Hg^{2+}	Fluorescence	21.7 nM	8.0–45 μM	This work

Fluorescence quenching concentration of Hg^{2+}; (e) Temperature of Hg^{2+} detection. Respective data and figures are deposited in the Electronic Supporting Material. The following experimental conditions were found to give the best results: (a) Sample pH 8.0, (b) The optimal fluorescence quenching and recovery reaction times are 8 min and 6 min, respectively, (c) The optimal concentration of g-CNQDs is 6.5 mg/L; (d) The optimal fluorescence quenching concentration of Hg^{2+} is 13.3 μM; (e) The working temperature of Hg^{2+} detection is 298 K.

"Turn-off" Hg^{2+} detection

The fluorescence behaviours of the prepared g-CNQDs toward different concentrations of Hg^{2+} were investigated. Figure 1a indicates that the fluorescence intensity of g-CNQDs is obviously reduced upon increasing the Hg^{2+} concentration, demonstrating the fluorescence "turn-off" detection of Hg^{2+}. The inset of Fig. 1a shows that the fluorescence intensity against the concentration of Hg^{2+} (0.20–21 μM) is linear and the limit of detection (LOD) is 3.3 nM. The linear equation is $1/(F_0–F_1) = 0.01018/C + 0.00117$ with the correlation coefficient (r) of 0.9999, where F_0 and F_1 are the fluorescence intensities of g-CNQDs in the absence and presence of Hg^{2+}, and C is the concentration of Hg^{2+}. The detection limit is based on the equation $LOD = 3\sigma/k$, where σ is the standard deviation of 11 replicate determinations of the blank g-CNQDs and k is the slope of the calibration plot.

A comparison of the detection limits and linear ranges of different methods for Hg^{2+}detection is shown in Table 1. It reveals that although several reported methods have lower LODs, our proposed method is still comparable to most other methods. But our materials for synthesizing g-CNQDs are relatively green and environmentally.

"Turn-on" sulfide detection

Since Hg^{2+} has a great affinity towards S^{2-} [32, 33], their strong coordination can recover the quenched fluorescence

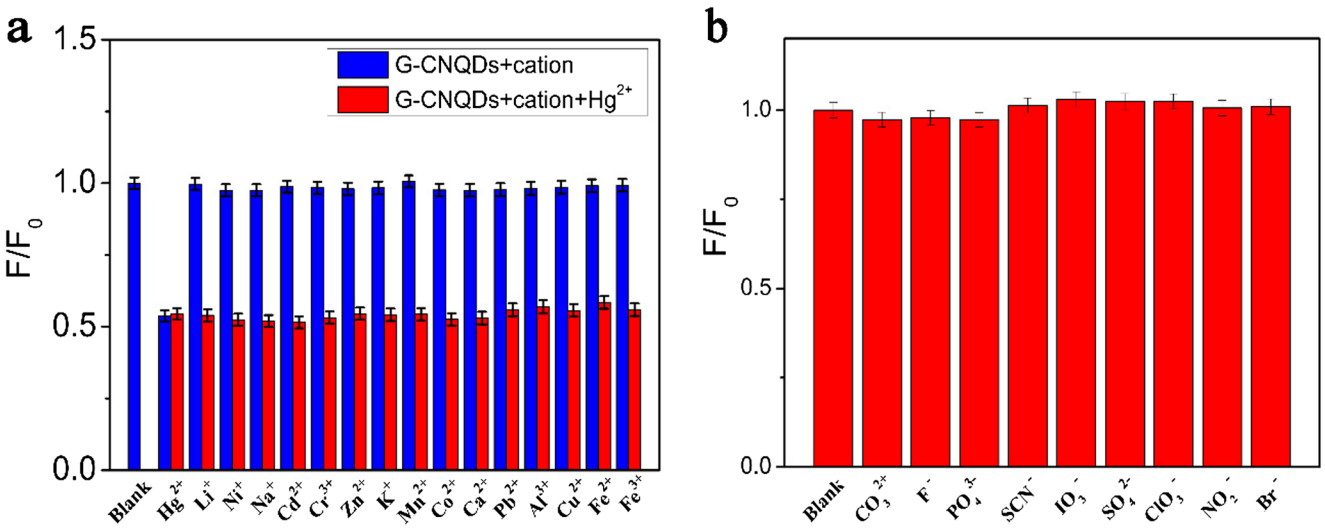

Fig. 2 **a** The response of g-CNQDs and Hg^{2+} in the absence and presence of other cations. **b** Fluorescence response of g-CNQDs-Hg^{2+} in the presence of different anions. The concentrations of ions are 100 μM

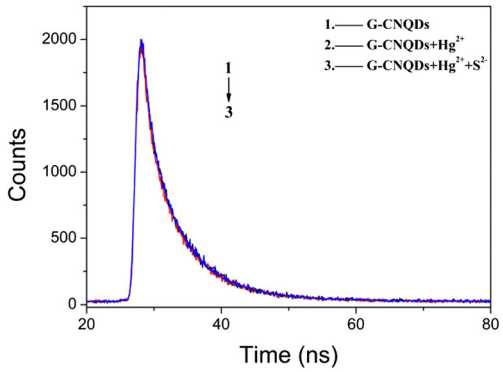

Fig. 3 Time-resolved fluorescence spectra of g-CNQDs, g-CNQDs-Hg^{2+}, and g-CNQDs-Hg^{2+}-S^{2-}

of g-CNQDs. Owing to the phenomenon of fluorescence recovery, g-CNQDs-Hg^{2+} system can be employed for sensitive and selective detection of S^{2-}. The fluorescence recovery response of g-CNQDs-Hg^{2+} system was analysed at different concentrations of S^{2-} under the optimal experimental conditions. The fluorescence intensity of g-CNQDs is recovered gradually with increasing the S^{2-} concentration. A linear relationship is established between the g-CNQDs fluorescence intensity and the concentration of S^{2-} ranging 8.0–45 μM (Inset: Fig. 1b) and the LOD is found to be 21.7 nM toward S^{2-}, where LOD is determined from $3\sigma/k$ with σ as the standard deviation of 11 replicate determinations of the g-CNQDs-Hg^{2+} and k as the slope of the calibration plot. The linear equation for S^{2-} is $F_2/F_1 = 0.02782C + 0.7516$, where F_1 and F_2 are the fluorescence intensities in the absence and presence of S^{2-}, respectively. The linear range and LOD for S^{2-} of this work are compared with other methods and displayed in Table 2. It can be seen that the LOD of our work is better than most other methods, and its sensitivity is good enough to detect sulfide in real water samples.

Selectivity study

To further verify the applicability of the fluorescence probe for detecting Hg^{2+} and S^{2-} in practical applications, the effect of common ions was investigated. Figure 2a represents the interference of different cations to Hg^{2+} detection. In the control experiment, the concentrations of Hg^{2+} and each cation were 3.0 and 100.0 μM, respectively. Those cations have negligible interference on the quenching fluorescence of g-CNQDs by Hg^{2+}. These results suggest that the g-CNQDs fluorescence probe for Hg^{2+} has high selectivity.

Analyses were carried out to investigate the interference effects of common anions on the recovery of g-CNQDs by S^{2-} in Fig. 2b. The concentration of S^{2-} and each anion were 10.0 and 100.0 μM, respectively. No significant change is observed in comparison to the blank. As such, the g-CNQDs-Hg^{2+} system is suitable for analysis of S^{2-} in the presence of other anions.

Mechanism analysis

Fluorescence quenching usually originates from static and/or dynamic quenching. Static quenching involves the formation of the complex by combining the ground state photoluminescent molecule with the quencher, while dynamic quenching refers to the collision of excited photoluminescent molecule with the quencher [48, 49]. In general, the static and dynamic quenching process can be analysed by Lineweaver-Burk equation Eq. (1) and Stern-Volmer equation Eq. (2), respectively:

$$\frac{1}{F_0 - F} = \frac{1}{F_0} + \frac{1}{F_0 K_{LB} C_q} \quad (1)$$

$$\frac{F_0}{F} = 1 + K_{SV} C_q \quad (2)$$

where F_0 and F are the fluorescence intensities of the fluorescence molecule with and without the quencher, respectively. C_q is the quencher concentration. K_{LB} is the Lineweaver-Burk constant and K_{SV} is the Stern-Volmer quenching constant. The Lineweaver-Burk plot can be used to determine if there is a linear relationship between the concentration of the metal ion of interest (Hg^{2+}) and the change of fluorescence intensity. K_{LB} is the static quenching constant, reflecting the efficiency of quenching or the accessibility of the fluorophores to the quencher. The sensitivity of the determination is directly related to the K_{LB} value [50]. The fluorescence quenching of g-

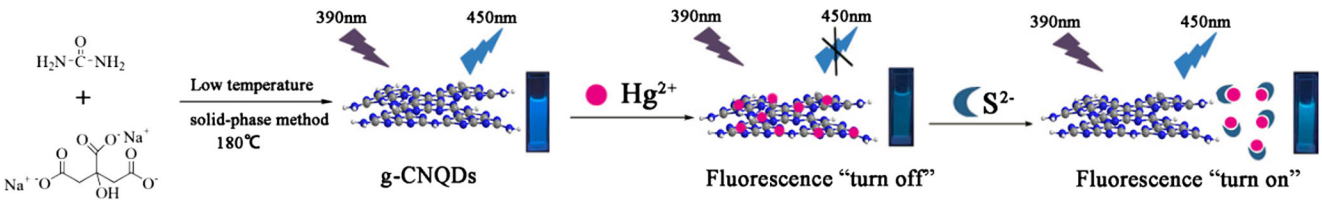

Scheme 1 Schematic illustration of detection of Hg^{2+} and S^{2-}

Table 3 Analytical results of Hg^{2+} in water samples

Samples	Added (μM)	Found (μM)	Recovery (%)	RSD (%)
Tap water	1.00	0.99	99.0	3.69
	9.00	9.80	108.8	4.01
	18.00	19.80	110.0	2.87
Lake water	1.00	1.00	100.0	4.45
	9.00	9.46	105.1	3.12
	18.00	18.41	102.3	2.02
Wastewater	1.00	1.10	110.0	3.68
	9.00	9.22	102.4	4.01
	18.00	18.24	101.3	3.87

CNQDs by Hg^{2+} ion fits well with the Lineweaver-Burk equation as displayed in the inset of Fig. 1a. Fig. S10 shows that the absorption peak of g-CNQDs at 390 nm gradually decreases with the increase in Hg^{2+} concentration, suggesting that static quenching may play a major role in the interaction of Hg^{2+} with g-CNQDs. In addition, the fluorescence lifetimes of g-CNQDs in the presence of various concentrations of Hg^{2+} were investigated as depicted in Fig. 3. There is no change of the g-CNQDs lifetime, inferring that the quenching process may be governed by the static mechanism.

There are lots of amino and hydroxyl groups on the surface of g-CNQDs. The selectivity and specificity of g-CNQDs to Hg^{2+} can probably attributed to the interaction between Hg^{2+} and the imine "N" (-C=N-C) or hydroxyl groups of g-CNQDs, making g-CNQDs to come close with each other and leading to a decrease of g-CNQDs fluorescence [51–53]. Thus, g-CNQDs can act as a "turn-off" fluorescent probe for Hg^{2+}. On the other hand, the fluorescence recovery of g-CNQDs-Hg^{2+} system by adding S^{2-} is ascribed to the competitive binding of S^{2-} with Hg^{2+}. S^{2-} can extract Hg^{2+} from g-CNQDs surface to form a stable complex, resulting in the fluorescence "turn-on" of g-CNQDs. In this way, the g-CNQDs-Hg^{2+} system can function as a "turn-on" probe for S^{2-}. The mechanism of the 'off-on' process is illustrated in Scheme 1.

Table 4 Analytical results of S^{2-} in water samples

Samples	Added (μM)	Found (μM)	Recovery (%)	RSD (%)
Tap water	10.00	9.80	98.0	3.70
	20.00	21.11	105.5	4.11
	30.00	29.67	98.9	3.67
Lake water	10.00	10.30	103.0	3.15
	20.00	21.71	108.5	3.92
	30.00	29.73	99.1	4.12
Wastewater	10.00	11.00	110.0	4.11
	20.00	20.49	102.5	4.02
	30.00	30.93	103.1	3.98

Analysis of Hg^{2+} and S^{2-} in water samples

The g-CNQDs probe was applied for analysis of Hg^{2+} and S^{2-} in water samples. Different concentrations of Hg^{2+} (1.00, 9.00, and 18.00 μM) were added to tap water, lake water and wastewater samples. The recovery of water samples ranges from 99.0 to 110.0% as depicted in Table 3. The relative standard deviation (RSD) is less than 5%, suggesting that the analytical performance for the detection of Hg^{2+} in water samples is satisfactory. Moreover, spiked water samples of various concentrations of S^{2-} (10.00, 20.00, and 30.00 μM) were also measured and the results are shown in Table 4. The recovery ranges from 98.0 to 110.0%, and the RSD is less than 5%. These results indicate that g-CNQDs may be a promising probe in real samples.

Biomatter, such as microorganism and substance produced by them, in wastewater may absorb UV light, which may display background fluorescence under UV excitation. Therefore, wastewater samples need to be pretreated before detecting ions, for instance, boiling and microfiltration. The pretreatment of water samples may bring inconvenience to detection. In brief, this method has some limitations. The fluorescence probe may not be suitable for biological samples owing to the need for working in the UV excitation.

Conclusion

In this work, a probe for the analyses of Hg^{2+} and S^{2-} is described. It is based on the "turn off-on" fluorescence phenomenon of g-CNQDs. Hg^{2+} induces significant fluorescence quenching of g-CNQDs. On the other hand, Hg^{2+} combines with sulfide and thereby recovers the fluorescence of g-CNQDs. The fluorescence 'off-on' probe enables rapid detection of Hg^{2+} and S^{2-} with high sensitivity and selectivity. This probe has been applied to various spiked water samples to detect Hg^{2+} and S^{2-} with satisfactory results. It is believed that the present strategy may offer a new approach for developing rapid, low-cost, highly sensitive and selective probe for real sample analyses.

Acknowledgements This work was supported by the Natural Science Foundation of Shanxi Province of China (201601D011018), PhD Start-up Foundation of Shanxi Medical University (03201514), Shanxi Medical University of Science and Technology Innovation Fund (01201312), and College Students'Innovative Entrepreneurial Training Project of Shanxi Medical University (20162202), Graduate Education Innovation Project of Shanxi Medical University (2018SY055) and 331 Early Career Research Grant of Basic Medical College of Shanxi Medical University (201417).

Compliance with ethical standards The author(s)declare that they have no competing interests.

References

1. Eagles-Smith CA, Silbergeld EK, Basu N, Bustamante P, Diaz-Barriga F, Hopkins WA, Kidd KA, Nyland JF (2018) Modulators of mercury risk to wildlife and humans in the context of rapid global change. Ambio 47(2):170–197. https://doi.org/10.1007/s13280-017-1011-x
2. Manavi PN, Mazumder A (2018) Potential risk of mercury to human health in three species of fish from the southern Caspian Sea. Mar Pollut Bull 130:1–5. https://doi.org/10.1016/j.marpolbul.2018.03.004
3. Pan S, Feng C, Lin J, Cheng L, Wang C, Zuo Y (2017) Occurrence and photodegradation of methylmercury in surface water of wen-Rui-Tang River network, Wenzhou, China. Environ Sci Pollut Res Int 24(12):11289–11298. https://doi.org/10.1007/s11356-017-8708-z
4. Deng L, Wu F, Deng N, Zuo Y (2008) Photoreduction of mercury(II) in the presence of algae, Anabaena cylindrical. J Photochem Photobiol B 91(2–3):117–124. https://doi.org/10.1016/j.jphotobiol.2008.02.005
5. Zuo Y, Pang S (1985) Determination of dialkyl mercury mompounds by reaction gas chromatography. Anal Chem 13: 890–895
6. Zuo Y, Pang S (1985) Photochemical methylation of inorganic mercury in the presence of sulfhydryl compounds. Acta Sci Circumst 5:239–243
7. Kenessary D, Kenessary A, Kenessariyev UI, Juszkiewicz K, Amrin MK, Erzhanova AE (2017) Human health cost of hydrogen sulfide air pollution from an oil and gas field. Ann Agr Env Med 24(2):213–216. https://doi.org/10.26444/aaem/74562
8. Muriel-García M, Cerón-Bretón RM, Cerón-Bretón JG (2016) Potential effects on human health of hydrogen sulfide exposure in a place in southeast of Mexico. J Ecol 06(01):47–54. https://doi.org/10.4236/oje.2016.61005
9. Omer KM, Mohammad NN, Baban SO, Hassan AQ (2018) Carbon nanodots as efficient photosensitizers to enhance visible-light driven photocatalytic activity. J Photochem Photobiol A Chem 364:53–58. https://doi.org/10.1016/j.jphotochem.2018.05.041
10. Gao G, Jiang Y-W, Jia H-R, Yang J, Wu F-G (2018) On-off-on fluorescent nanosensor for Fe^{3+} detection and cancer/normal cell differentiation via silicon-doped carbon quantum dots. Carbon 134:232–243. https://doi.org/10.1016/j.carbon.2018.02.063
11. Kalaiyarasan G, Joseph J (2017) Determination of vitamin B12 via pH-dependent quenching of the fluorescence of nitrogen doped carbon quantum dots. Microchim Acta 184(10):3883–3891. https://doi.org/10.1007/s00604-017-2421-y
12. Omer KM, Hassan AQ (2017) Chelation-enhanced fluorescence of phosphorus doped carbon nanodots for multi-ion detection. Microchim Acta 184(7):2063–2071. https://doi.org/10.1007/s00604-017-2196-1
13. Dong Y, Wang Q, Wu H, Chen Y, Lu CH, Chi Y, Yang HH (2016) Graphitic carbon nitride materials: sensing, imaging and therapy. Small 12(39):5376–5393. https://doi.org/10.1002/smll.201602056
14. Wang A, Wang C, Fu L, Wong-Ng W, Lan Y (2017) Recent advances of graphitic carbon nitride-based structures and applications in catalyst, sensing, imaging, and LEDs. Nano-Micro Lett 9(4). https://doi.org/10.1007/s40820-017-0148-2
15. Von Liebig J (1834) Uber einige stickstoff-verbindungen. Eur J Org Chem 10(1):1–47. https://doi.org/10.1002/jlac.18340100102
16. Liu AY, Cohen ML (1989) Prediction of new low compressibility solids. Science 245(4920):841–842. https://doi.org/10.1126/science.245.4920.841
17. Wang X, Maeda K, Thomas A, Takanabe K, Xin G, Carlsson JM, Domen K, Antonietti M (2009) A metal-free polymeric photocatalyst for hydrogen production from water under visible light. Nat Mater 8(1):76–80. https://doi.org/10.1038/nmat2317
18. Wang X, Maeda K, Chen X, Takanabe K, Domen K, Hou Y, Fu X, Antonietti M (2009) Polymer semiconductors for artificial photosynthesis: hydrogen evolution by mesoporous graphitic carbon nitride with visible light. J Am Chem Soc 131:1680–1681. https://doi.org/10.1021/ja809307s
19. Lan D-H, Wang H-T, Chen L, Au C-T, Yin S-F (2016) Phosphorous-modified bulk graphitic carbon nitride: facile preparation and application as an acid-base bifunctional and efficient catalyst for CO 2 cycloaddition with epoxides. Carbon 100:81–89. https://doi.org/10.1016/j.carbon.2015.12.098
20. Yuan X, Zhou C, Jin Y, Jing Q, Yang Y, Shen X, Tang Q, Mu Y, Du AK (2016) Facile synthesis of 3D porous thermally exfoliated g-C3N4 nanosheet with enhanced photocatalytic degradation of organic dye. J Colloid Interface Sci 468:211–219. https://doi.org/10.1016/j.jcis.2016.01.048
21. Yuan H, Liu J, Li H, Li Y, Liu X, Shi D, Wu Q, Jiao Q (2018) Graphitic carbon nitride quantum dot decorated three-dimensional graphene as an efficient metal-free electrocatalyst for triiodide reduction. J Mater Chem A 6(14):5603–5607. https://doi.org/10.1039/c8ta00205c
22. Zhai S, Guo P, Zheng J, Zhao P, Suo B, Wan Y (2018) Density functional theory study on the stability, electronic structure and absorption spectrum of small size g-C 3 N 4 quantum dots. Comput Mater Sci 148:149–156. https://doi.org/10.1016/j.commatsci.2018.02.023
23. Wu J, Yang S, Li J, Yang Y, Wang G, Bu X, He P, Sun J, Yang J, Deng Y, Ding G, Xie X (2016) Electron injection of phosphorus doped g-C3N4 quantum dots: controllable photoluminescence emission wavelength in the whole visible light range with high quantum yield. Adv Optical Mater 4(12):2095–2101. https://doi.org/10.1002/adom.201600570
24. Achadu OJ, Nyokong T (2017) In situ one-pot synthesis of graphitic carbon nitride quantum dots and its 2,2,6,6-tetramethyl (piperidin-1-yl)oxyl derivatives as fluorescent nanosensors for ascorbic acid. Anal Chim Acta 991:113–126. https://doi.org/10.1016/j.aca.2017.07.047
25. Yin Y, Zhang Y, Gao T, Yao T, Han J, Han Z, Zhang Z, Wu Q, Song B (2017) One-pot evaporation–condensation strategy for green synthesis of carbon nitride quantum dots: an efficient fluorescent probe for ion detection and bioimaging. Mater Chem Phys 194:293–301. https://doi.org/10.1016/j.matchemphys.2017.03.054
26. Wang H, Ma Q, Wang Y, Wang C, Qin D, Shan D, Chen J, Lu X (2017) Resonance energy transfer based electrochemiluminescence and fluorescence sensing of riboflavin using graphitic carbon nitride quantum dots. Anal Chim Acta 973:34–42. https://doi.org/10.1016/j.aca.2017.03.041
27. Zhou J, Yang Y, Zhang CY (2013) A low-temperature solid-phase method to synthesize highly fluorescent carbon nitride dots with tunable emission. Chem Commun (Camb) 49(77):8605–8607. https://doi.org/10.1039/c3cc42266f
28. Weng H, Yan B (2017) A Eu(III) doped metal-organic framework conjugated with fluorescein-labeled single-stranded DNA for detection of cu(II) and sulfide. Anal Chim Acta 988:89–95. https://doi.org/10.1016/j.aca.2017.07.061
29. Chai L-Y, Wang Q-W, Wang Y-Y, Li Q-Z, Yang Z-H, Shu Y-D (2010) Thermodynamic study on reaction path of hg(II) with S(II) in solution. J Cent S Univ Technol 17:289–294. https://doi.org/10.1007/s11771-010-0044-0

30. Elliott S (1988) Linear free energy techniques for estimation of metal sulfide complexation constants. Mar Chem 24:203–213
31. Bi N, Hu M, Xu J, Jia L (2017) Colorimetric determination of mercury(II) based on the inhibition of the aggregation of gold nanorods coated with 6-mercaptopurine. Microchim Acta 184(10): 3961–3967. https://doi.org/10.1007/s00604-017-2427-5
32. Hong M, Zeng B, Li M, Xu X, Chen G (2017) An ultrasensitive conformation-dependent colorimetric probe for the detection of mercury(II) using exonuclease III-assisted target recycling and gold nanoparticles. Microchim Acta 185(1):72. https://doi.org/10.1007/s00604-017-2536-1
33. Zhang R, Deng L, Zhu P, Xu S, Huang C, Zeng Y, Ni S, Zhang X (2016) Bienzyme-based visual and spectrophotometric aptamer assay for quantitation of nanomolar levels of mercury(II). Microchim Acta 184(2):541–546. https://doi.org/10.1007/s00604-016-2033-y
34. Lu Y, Zhong J, Yao G, Huang Q (2018) A label-free SERS approach to quantitative and selective detection of mercury (II) based on DNA aptamer-modified SiO2@au core/shell nanoparticles. Sensors Actuators B Chem 258:365–372. https://doi.org/10.1016/j.snb.2017.11.110
35. Jayadevimanoranjitham J, Narayanan SS (2018) 2,4,6-Trimercaptotriazine incorporated gold nanoparticle modified electrode for anodic stripping voltammetric determination of hg(II). Appl Surf Sci 448:444–454. https://doi.org/10.1016/j.apsusc.2018.04.096
36. Xu S, Liu Y, Yang H, Zhang K, Li J, Deng A (2017) Fluorescent nitrogen and sulfur co-doped carbon dots from casein and their applications for sensitive detection of Hg^{2+} and biothiols and cellular imaging. Anal Chim Acta 964:150–160. https://doi.org/10.1016/j.aca.2017.01.037
37. Ding X, Qu L, Yang R, Zhou Y, Yang J, Li J (2015) A highly selective and simple fluorescent sensor for mercury (II) ion detection based on cysteamine-capped CdTe quantum dots synthesized by the reflux method. Luminescence 30:465–471. https://doi.org/10.1002/bio.2761
38. Zhang J, Yu SH (2014) Highly photoluminescent silicon nanocrystals for rapid, label-free and recyclable detection of mercuric ions. Nanoscale 6:4096–4101. https://doi.org/10.1039/c3nr05896d
39. Wang B, Zhuo S, Chen L, Zhang Y (2014) Fluorescent graphene quantum dot nanoprobes for the sensitive and selective detection of mercury ions. Spectrochim Acta A Mol Biomol Spectrosc 131(19): 384–387. https://doi.org/10.1016/j.saa.2014.04.129
40. Butwong N, Srijaranai S, Luong J (2016) Fluorometric determination of hydrogen sulfide via silver-doped CdS quantum dots in solution and in a test strip. Microchim Acta 183:1243–1249. https://doi.org/10.1007/s00604-016-1755-1
41. Ni P, Chen C, Jiang Y, Zhao Z, Lu Y (2018) Fluorometric determination of sulfide ions via its inhibitory effect on the oxidation of thiamine by cu(II) ions. Microchim Acta 185(8):362. https://doi.org/10.1007/s00604-018-2906-3
42. Deng HH, Weng SH, Huang SL, Zhang LN, Liu AL, Lin XH, Chen W (2014) Colorimetric detection of sulfide based on target-induced shielding against the peroxidase-like activity of gold nanoparticles. Anal Chim Acta 852:218–222
43. Jin LH, Zhang ZH, Tang AW, Li C, Shen YH (2016) Synthesis of yeast extract-stabilized cu nanoclusters for sensitive fluorescent detection of sulfide ions in water. Biosens Bioelectron 79:108–113
44. Li ZH, Guo S, Lu C (2015) A highly selective fluorescent probe for sulfide ions based on aggregation of cu nanocluster induced emission enhancement. Analyst 140:2719–2725
45. Gore AH, Vatre SB, Anbhule PV, Han SH, Patil SR, Kolekar GB (2013) Direct detection of sulfide ions [S^{2-}] in aqueous media based on fluorescence quenching of functionalized CdS QDs at trace levels: analytical applications to environmental analysis. Analyst 138:1329–1333. https://doi.org/10.1039/c3an36825d
46. Zhang B-H, Wu F-Y, Wu Y-M, Zhan X-S (2010) Fluorescent method for the determination of sulfide anion with ZnS:Mn quantum dots. J Fluoresc 20:243–250. https://doi.org/10.1007/s10895-009-0545-0
47. Rajabi HR, Shamsipur M, Khosravi AA, Khani O, Yousefi MH (2013) Selective spectrofluorimetric determination of sulfide ion using manganese doped ZnS quantum dots as luminescent probe. Spectrochim Acta A Mol Biomol Spectrosc 107:256–262. https://doi.org/10.1016/j.saa.2013.01.045
48. Akram M, Ansari F, Bhat IA, Chaturvedi SK, Khan RH, Kabir ud D (2017) Analyzing the interaction between porcine serum albumin (PSA) and ester-functionalized cationic gemini surfactants. Process Biochem 63:145–153. https://doi.org/10.1016/j.procbio.2017.07.026
49. Rabbani G, Baig MH, Jan AT, Ju Lee E, Khan MV, Zaman M, Farouk AE, Khan RH, Choi I (2017) Binding of erucic acid with human serum albumin using a spectroscopic and molecular docking study. Int J Biol Macromol 105(Pt 3):1572–1580. https://doi.org/10.1016/j.ijbiomac.2017.04.051
50. Joseph RL (2006) Principles of fluorescence spectroscopy. University of Maryland School of Medicine Baltimore, Maryland, USA
51. Kim H-S, Angupillai S, Jeong Y-M, Park J-S, Kim C-H, Son Y-A (2017) Through-bond energy transfer based dyad and triad shape fluorescence "OFF-ON-OFF" probes for Hg^{2+} ions and their application in live HeLa cells and zebrafish. Sensors Actuators B Chem 240:1272–1282. https://doi.org/10.1016/j.snb.2016.09.115
52. Lu W, Qin X, Liu S, Chang G, Zhang Y, Luo Y, Asiri AM, Al-Youbi AO, Sun X (2012) Economical, green synthesis of fluorescent carbon nanoparticles and their use as probes for sensitive and selective detection of mercury(II) ions. Anal Chem 84(12):5351–5357. https://doi.org/10.1021/ac3007939
53. Guo Y, Wang Z, Shao H, Jiang X (2013) Hydrothermal synthesis of highly fluorescent carbon nanoparticles from sodium citrate and their use for the detection of mercury ions. Carbon 52:583–589. https://doi.org/10.1016/j.carbon.2012.10.028